Research Article | **Open Access**

Investigation of Optical and Dielectric Constants of Organic-Inorganic CH$_3$NH$_3$PbI$_3$ Perovskite Thin Films

Yang A[1]*, Bai M[1], Bao X[2], Wang J[2] and Zhang W[1]

[1]Department of Physics, Ocean University of China, Qingdao, 266100, PR China
[2]Qingdao Institute of Bioenergy & Bioprocess Technology, Chinese Academy of Sciences, Qingdao, 266101, China

Abstract

CH$_3$NH$_3$PbI$_3$ thin films with thicknesses in the region of 230-365 nm were prepared. The films were characterized by scanning electron microscope (SEM), x-ray diffraction (XRD), ultraviolet-visible (UV-Vis) absorption and transmittance spectra. Based on the Kramers-Kronig relation and the transmittance spectra, the optical and dielectric constants of the CH$_3$NH$_3$PbI$_3$ thin films were investigated. Our results show that the absorption coefficient, extinction coefficient, refractive indices, real and imaginary components of the dielectric constant of the CH$_3$NH$_3$PbI$_3$ films are basically independent on the thicknesses of the films, which indicate our results are reliable. At 500 nm, above parameters of the films are ~ 1.38x10^5 cm^{-1}, 0.55, 2.70, 7.01, and 3.13, respectively. The band gap is 1.595 eV. The refractive index of CH$_3$NH$_3$PbI$_3$ thin films is 2.84 at 633 nm, which imply that CH$_3$NH$_3$PbI$_3$-based solar cells (SCs) are ideal antireflection coatings for silicon SCs and are applicable to be top SC in monolithic silicon-based tandem SCs for beyond the efficiency limit of Si SCs. Our results are meaningful for designing optoelectronic devices related to the perovskite thin-films.

Keywords: CH$_3$NH$_3$PbI$_3$ perovskite thin films; optical constants; Kramers-kronig relation

Introduction

Organic-inorganic pervoskite of CH$_3$NH$_3$PbX$_3$ (X=Cl, Br, I) families have attracted extreme attention as light-harvesting materials in SCs. Within past six years, power conversion efficiency of pervoskite SCs has been enhanced from 3.8% [1] to 20.1% [2], which is the fastest increasing rate in the history of SCs. The impressive photovoltaic efficiency of perovskite SCs attribute to their unique optical and electrical properties, such as an appropriate band gap (1.50 eV) [2,3], high absorption coefficient [2,4], high open-circuit voltages (1.3 V) [5], long hole-electron diffusion length (~100 nm) and excellent carrier transportation [6]. The quality of perovskite films is very important for SCs. A variety approaches have been employed to fabricate perovskite films, such as single step solution method [7-9], sequential deposition of inorganic and organic precursor [10], co-evaporation of the precursors [11] and vapor assistant solution process [12].

Except for perovskite SCs, organic-inorganic perovskite are also promising materials for light-emitting diodes [13], lasers [14] and thin-film electronic devices [15]. For designing thin-film optoelectronic devices, optical parameters such as absorption coefficient, extinction coefficient, refractive index, optical band gap and dielectric coefficient are very important parameters.

So far, the optical and dielectric properties of CH$_3$NH$_3$PbI$_3$ thin film have been little studied. Hirasawa et al. [16] obtained the dielecttric constant of 6.5 in visible range at temperature of 4.2 K. Stefaan De Wolf et al. [4] found a high absorption coefficient with particularly sharp onset by photothermal deflection and photocurrent spectroscopy. Xie Zhang et al. [17] fabricated the CH$_3$NH$_3$PbI$_3$ thin films by dualsource evaporation technique and studied the refractive index and extinction coefficient of CH$_3$NH$_3$PbI$_3$ layer by spectroscopic ellipsometry in the range of 300-2000 nm, the refractive index of CH$_3$NH$_3$PbI$_3$ thin film is of 2.8-3.4 in the visible range, and almost a constant (2.6) in near-infrared range. Philipp Loper et al. [18] investigated the complex refractive index of planar CH$_3$NH$_3$PbI$_3$ thin films at room temperature by variable angle spectroscopic ellipsometry and spectrophotometry. The authors modeled the dielectric function according to the Forouhi-Bloomer formulation. In the visible range, the refractive index of

CH$_3$NH$_3$PbI$_3$ thin film is of 2.5-2.8, and in near-infrared range, the refractive index is 2.3-2.6. Qianqian Lin et al. [19] achieved the refractive index and extinction coefficient in the visible to near-infrared wavelength range by a combination of spectroscopic ellipsometry, total transmittance and near-normal incidence reflectance measurements. The refractive index is 2.5-3.2. There are two peaks at 510 nm and 775 nm with refractive index of 3.2 and 2.8 respectively. Chang-Wen Chen et al. [20] determined the refractive index and extinction coefficient of CH$_3$NH$_3$PbI$_{3-x}$Cl$_x$ single sample by using a combination of reflection and transmission ellipsometric measurements, which eliminates the risk of sample to sample variation that could occur in a multi-sample analysis. And the refractive index is approximately 2.4-2.6 in the visible to near-infrared wavelength range. The films show extinction coefficient peaks at 355 nm, 460 nm, 630 nm and 730 nm with extinction coefficient values of 1.29, 0.75, 0.30 and 0.26, respectively. From the published results about the refractive index and extinction coefficient of CH$_3$NH$_3$PbI$_3$ perovskite films we can see that different research groups obtained different data. The main reasons are reflection and transmission ellipsometric measurements are different for the samples with different film quality.

In this paper, high-quality CH$_3$NH$_3$PbI$_3$ perovskite films with different thicknesses were prepared. The features of the films were characterized by SEM, XRD, UV-Vis absorption and transmittance spectra. Based on the Kramers-Kronig relation [21-23] and the transmittance spectra, the optical and dielectric constants of the CH$_3$NH$_3$PbI$_3$ perovskite films were calculated. Our results show that the band gap of the films, absorption coefficient, extinction coefficient,

refractive indices, real and imaginary components of the dielectric constant of the $CH_3NH_3PbI_3$ films are basically independent on the thicknesses, which indicate our results are reliable.

Experiment

Materials and characterization

Methylamine (33 wt% in ethanol), hydroiodic acid (57 wt% in water), PbI_2, N, N-Dimethylformamide (DMF), and diethyl ether were purchased from Aladdin reagent, Shanghai, China. γ-Butyrolactone (GBL), dimethylsulphoxide (DMSO), N-methyl-2-pyrrolidone (NMP) were also purchased from Aladdin reagent. The above materials were used as received. The morphology of $CH_3NH_3PbI_3$ films was characterized by SEM (Hi-tachi4800). The XRD pattern was obtained on a Bruker D8 ADVANCE instrument (Billerica, MA). A Lamda-25 UV-Vis spectrophotometer was used to measure the absorption and transmission spectra. The thicknesses of the films were measured by a Veeco Dektak150 surface profiler.

Fabrication of the $CH_3NH_3PbI_3$ films

The fabrication of $CH_3NH_3PbI_3$ films is similar to our previous method [24] with a small change. Under argon at 0°C, CH_3NH_3I was synthesized by methylamine (36 mL) and hydroiodic acid (15 mL) reacting in 150 mL ethanol for 2 h. The white precipitate of CH_3NH_3I was gained by rotary evaporation at 50°C then dissolved in ethanol followed by sedimentation in diethyl ether under stirring the solution for 30 min. Above steps were repeated three times and the white CH_3NH_3I powder was finally collected and dried at 50°C in a vacuum oven overnight. The CH_3NH_3I and PbI_2 (1 M) were dissolved in a mixture of anhydrous GBL: DMSO (7:3), with 5 v/v% NMP. To strengthen dissolution of solid material, the solution was heated at 70°C overnight, then cooled down to room temperature and act as a precursor solution of the films. Before spin-coating, the precursor solution was filtered with a 0.22 mm PTFE filter. ITO glasses were as the substrates of the $CH_3NH_3PbI_3$ films. Before spin-coating, the ITO glasses were cleaned in an ultrasonic bath with detergent, ultrapure water, acetone, and isopropyl alcohol for 20 min, respectively. After being treated in oxygen plasma for 6 min, the precursor solution was spin-coated onto the ITO glasses. During the spin-coating, toluene was used to wash the surface to form high-quality surface coverage, as reported by Seok [7] and Bao [24]. Finally, the films were thermal treated at 90 °C for 20 min in a glovebox. By adjust the rotating speed, $CH_3NH_3PbI_3$ films with 230 nm, 260 nm, 295 nm and 365 nm thicknesses were prepared. The experimental error in measuring the film thickness is about 5 nm.

Characterization of the films

Figure 1 shows the representative SEM image. We can see that the $CH_3NH_3PbI_3$ thin film on the ITO coated glass is composed of uniform grains. The perovskite film fully covered on the ITO layer without any cracks, pinholes and other serious aggregations. The quality of the film is good.

Figure 2 is the XRD pattern of $CH_3NH_3PbI_3$ thin film. The four main peaks located at 14.18°, 28.50°, 31.92°, 34.24° correspond to the lattice plane (110), (220), (310) and (312) respectively. It is similar to the result of Ref. 12. The peaks related to CH_3NH_3I and PbI_2 were not observed in the synthesized perovskite layer, which indicates CH_3NH_3I and PbI_2 completely reacted and transformed into $CH_3NH_3PbI_3$.

Figure 3 shows the UV-Vis absorption spectra of the four
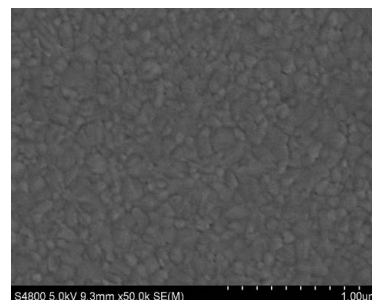
Figure 1: SEM image of $CH_3NH_3PbI_3$ thin film.
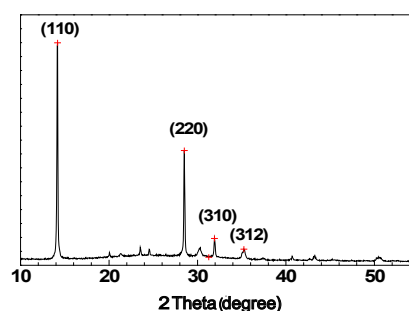
Figure 2: XRD pattern of $CH_3NH_3PbI_3$ thin film.
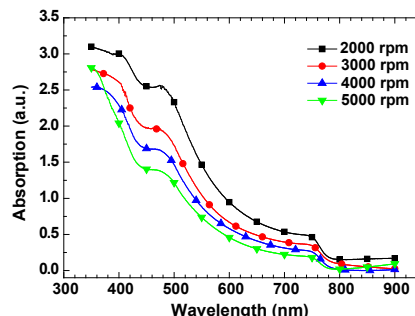
Figure 3: UV-Vis absorption spectra of the $CH_3NH_3PbI_3$ thin films.

$CH_3NH_3PbI_3$ thin films. The films have wide absorption range from UV to NIR regions with two distinct peaks positioned at 480 nm and 756 nm respectively. The first absorption peak (480 nm) is attributed to the direct gap transition from lower valence band (VB_2) to the conduction band minimum (CB_1), which is near to 2.58 eV [6,17]. And the second absorption peak (756 nm) is assigned to the direct gap transition from the first valence band maximum (VB_1) to the conduction band minimum (CB_1), which is approximate to 1.64 eV [6,17].

Figure 4 indicates the transmission curves of the four $CH_3NH_3PbI_3$ thin films. In the UV-Vis range, the thicker the films, the higher the transmittance. The transmittance of the films is less than 10% when the wavelength is less than 540 nm. In the range of 540-750 nm, the transmittance almost increases linearly from 10% to 30%. And in the region of 750-800 nm, the transmittance increases quickly near to 70%. The highest transmission is 76% at 800 nm for the film with 295 nm thickness. In the range of 800-1000 nm, the transmittance decrease

slightly. The change tendency is consistent with the experiment result reported by Philipp LÖper et al. [18].

Calculation and Discussion

The absorption coefficient $\alpha(\lambda)$ of the CH$_3$NH$_3$PbI$_3$ thin films can be calculated by the transmittance spectra as following equation [21],

$$T = \exp[-\alpha(\lambda)d] \tag{1}$$

where T is the transmittance and d is the thickness of thin film. Figure 5 shows the calculated results. From 320 nm to 775 nm, $\alpha(\lambda)$ exhibits independence on the film thicknesses. In the range of 310-510 nm, $\alpha(\lambda)$ are almost constant of 1.4×10^5 cm^{-1}. And in the range of 510-750 nm, $\alpha(\lambda)$ decrease from 1.4×10^5 cm^{-1} to 4×10^4 cm^{-1}. The absorption coefficient curves of CH$_3$NH$_3$PbI$_3$ films show a sharp shoulder near the wavelength of 756 nm, which corresponds to the position of the band gap. Our results coincide with Ref. 4. Comparison to GaAs, CdTe, CIGS and c-Si, this shoulder occurs at higher absorption coefficients [4]. So very thin absorber films are suffice for perovskite SCs fabrication [4]. In the NIR range of 756-800 nm, $\alpha(\lambda)$ decrease again till to the fundamental absorption edge. The magnitude of $\alpha(\lambda)$ and spectral shape are good agreement with previous reports [4,18].

The extinction coefficient $k(\lambda)$ can be calculated by below equation [21]:

$$\kappa(\lambda) = \frac{\alpha(\lambda)\lambda}{4\pi} \tag{2}$$

Figure 6 shows the curves of extinction coefficient of CH$_3$NH$_3$PbI$_3$ thin films. At 510 nm and 750 nm, the peaks of $k(\lambda)$ are near to 0.55 and 0.25 respectively. The values of $k(\lambda)$ in the visible regions are larger than that in the NIR regions. From 340 nm to 510 nm, $k(\lambda)$ increase with wavelengths till the peak value of 0.55 at 510 nm. In the range of 510-750 nm, $k(\lambda)$ decrease slowly down to 0.25. In the NIR range of 750-800 nm, $k(\lambda)$ decrease again and follow a linear trend till to 0.14 (230 nm thickness) and 0.05 (295 nm thickness). In the range of 800-850 nm, $k(\lambda)$ are almost constants and show dependence on the thickness of films.

The classical Tauc equation [25] was used to calculated the optical band gap E_g

$$\alpha(\lambda)h\nu = A\left(\frac{hc}{\lambda} - E_g\right)^m \tag{3}$$

Where A is a constant, h and c are the Planck's constant and light speed respectively. For the direct band gap semiconductor, m=1/2 or 2/3 [22]. When m=1/2, the calculated results gives the best linear plot in the band edge region for the CH$_3$NH$_3$PbI$_3$ thin films. Representative plots of $(\alpha h\nu)^2$ verses photon energy were showed in Figure 7. The band gap of CH$_3$NH$_3$PbI$_3$ thin films were obtained by extrapolation α to zero. For the four films with different thicknesses, the band gap is same (1.595 eV), which is almost as same as Ref. 2, Ref. 3 and Ref.17.

The refractive index $n(\lambda)$ and absorption coefficient $\alpha(\lambda)$ of a thin film are related by Kramers-Kronig equation [21,23],

$$n(\lambda) = 1 + \frac{1}{2\pi^2}\int_0^\infty \frac{\alpha(\lambda')d\lambda'}{1 - \lambda'^2/\lambda^2} \tag{4}$$

The integration range is from 0 to ∞, which means one has to know $\alpha(\lambda')$ in the range of $[0, \infty]$ for calculation the refractive index at λ. But from experimental transmittance spectrum, one can only obtain $\alpha(\lambda')$ in a limited wavelength range ($\lambda_1' \sim \lambda_2'$). In the regions of $\lambda' < \lambda_1'$ and $\lambda' > \lambda_2'$, one has to speculate $\alpha(\lambda')$. So Eq. (4) can be written as
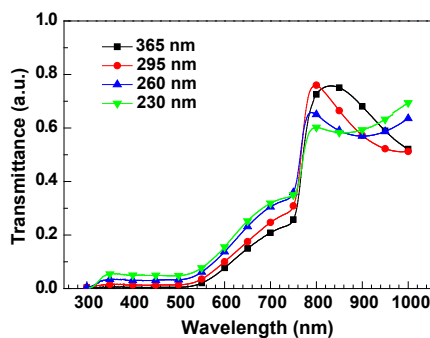
Figure 4: Transmittance spectra of CH$_3$NH$_3$PbI$_3$ thin films.
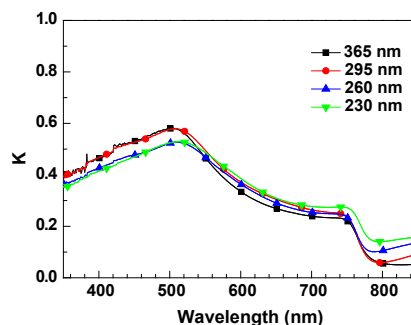
Figure 6: Extinction coefficients curve of the CH$_3$NH$_3$PbI$_3$ thin films.
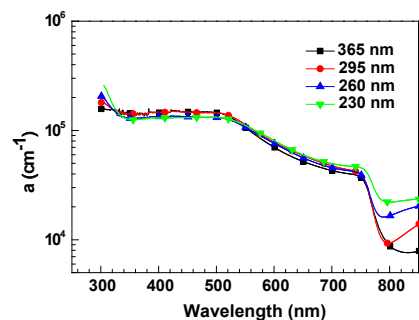
Figure 5: Absorption coefficients curves of the CH$_3$NH$_3$PbI$_3$ thin films.
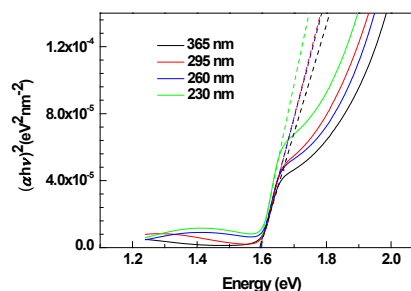
Figure 7: Plots of $(\alpha h\nu)^2$ vs E for direct transitions of CH$_3$NH$_3$PbI$_3$ thin films.
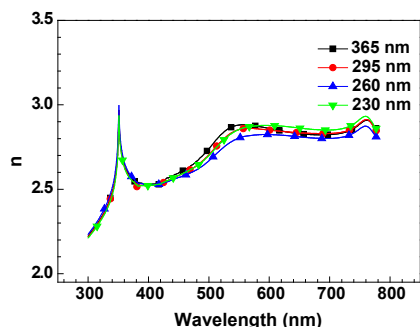
Figure 8: Refractive index curves of $CH_3NH_3PbI_3$ thin films.
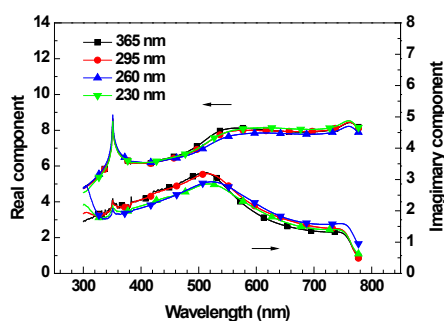
Figure 9: Real components and imaginary components of complex dielectric constant of $CH_3NH_3PbI_3$ thin films.

$$n(\lambda) = 1 + \sum_{i=1}^{3} j_i \qquad (5)$$

Where j_i ($i=1, 2$ and 3) are the integrations of Eq.(4) in the ranges of $\lambda' < \lambda_1'$, $\lambda_1' \sim \lambda_2'$ and $\lambda' > \lambda_2'$, respectively. At the short wavelength, we suppose that there is only one absorption band and $\alpha(\lambda')$ match Eq. (3) and m=1/2. By combining Eq. (4) and (3), j_1 can be written as the sum of the integration under three cases, $hc/\lambda' - E_g > 0$, $hc/\lambda' - E_g = 0$ and $hc/\lambda' - E_g < 0$. In Ref. 23, we corrected the equations to calculate j_1 in the above three cases and calculated the optical constants of ZnO nano-thin films. The same equations were used here to calculate j_1. The equations to calculate j_2 and j_3 are as same as Ref. 21.

Figure 8 shows the dependence of refractive indices on the wavelengths. There are three peaks of the refractive indices. One sharp peak with value of 3.0 is at 350 nm, which resembles the result of Ref. 17 and Ref.18. Another slowly change peak near to 2.84 is at 550 nm. There is a small peak at 760 nm. In the region of 350- 400 nm, the refractive indices decrease from 3.0 to 2.53, then increase to 2.84 at 550 nm. From 550 nm to 750 nm, the refractive index is almost a constant (around 2.8). At 633 nm, the refractive index of $CH_3NH_3PbI_3$ films is near to 2.8, which imply that $CH_3NH_3PbI_3$ is an ideal antireflection coating for silicon SCs. The tandem SCs of $CH_3NH_3PbI_3$/Si are promising to beyond the efficiency limit of Si SCs.

The complex dielectric $\varepsilon = \varepsilon_1 + i\varepsilon_2$ characterizes the optical properties of solid material. The real and imaginary parts of the complex dielectric constants are expressed as [21]:

$$\varepsilon_1 = n^2(\lambda) - \kappa^2(\lambda) \qquad (6)$$

$$\varepsilon_2 = 2n(\lambda)\kappa(\lambda) \qquad (7)$$

Figure 9 shows the real and imaginary components of the complex dielectric constants of $CH_3NH_3PbI_3$ thin films. The real components follow the same pattern as the refractive indices changing with wavelengths (Figure 8). There is a sharp peak at 350 nm. In the region of 300-350 nm, the real components ε_1 increase from 4.7 to 9.0, then decrease to 6.18 at 400 nm. In the region of 400-560 nm, ε_1 increase from 6.18 to 7.95. After 560 nm, ε_1 is almost a constant near to 8.0. Our result for the real components of the complex dielectric constants is in good agreement with Ref. 18. Hirasawa et al. [16] obtained the dielectric constant of 6.5 in visible range at temperature of 4.2 K. For the imaginary component ε_2, the peaks are at 350 nm and 510 nm. The first cuspidal peak at 350 nm resembles to the result of Ref. 18. In the region of 360-510 nm, ε_2 increase from 2.00 to the peak value of 3.03 at 510 nm then decrease down to 1.39 at 775 nm.

Conclusions

In this work, $CH_3NH_3PbI_3$ thin films with thicknesses in the range of 230-365 nm were prepared. The features of the films were characterized by SEM, XRD, UV-Vis absorption and transmittance spectra. The optical constants including in absorption coefficient, extinction coefficient, refractive indices, real and imaginary components of the dielectric constant were calculated based on the Kramers-Kronig relation. These optical and dielectric constants are basically independent on the thicknesses of the films, which indicate our results are reliable. At 500 nm, above parameters of the films are ~1.38×10^5 cm^{-1}, 0.55, 2.70, 7.01, and 3.13, respectively. Our results agree well with previously reported data. The band gap of the films is 1.595 eV. The real part of the refractive index at 633 nm is 2.84, which indicates that $CH_3NH_3PbI_3$-based SCs are applicable to top cell in monolithic silicon-based tandem SCs. Our results are meaningful for designing optoelectronic devices related to the perovskite thin-films.

References

1. Kojima A, Teshima K, Shirai Y, Miyasaka T (2009) Organometal halide perovskites as visible-light sensitizers for photovoltaic cells. J Am Chem Soc 131: 6050-6051.

2. Park NG (2015) Perovskite solar cells: an emerging photovoltaic technology. Mater Today 18: 65-72.

3. Kim HS, Lee CR, Im JH, Lee KB, Moehl T, et al. (2012) Lead iodide perovskite sensitized all-solide-state submicron thin film mesoscopic solar cell with efficiency exceeding 9%. Sci Rep-Uk 2: 591.

4. Wolf SD, Holovsky J, Moon SJ, Löper P, Niesen B, et al. (2014) Organometallic halide perovskites: Sharp optical absorption edge and its relation to photovoltaic performance. J Phys Chem Lett 5: 1035-1039.

5. Edri E, Kirmayer S, Cahen D, Hodes G (2013) High open-circuit voltage solar cells based on organic-inorganic lead bromide perovskite. J Phys Chem Lett 4: 897-902.

6. Xing G, Mathews N, Sun S, Lim SS, Lam YM, et al. (2013) Long-range balanced electron-and hole-transport lengths in organic-inorganic $CH_3NH_3PbI_3$. Science 342: 344-347.

7. Jeon NJ, Noh JH, Kim YC, Yang WS, Ryu WS, et al. (2014) Solvent engineering for high-performance inorganic-organic hybrid perovskite solar cells. Nat Mater 13: 897-903.

8. Liu D, Kelly TL (2014) Perovskite solar cells with a planar heterojunction structure prepared using room-temperature solution processing techniques. Nat photonics 8:133-138.

9. Zhou H, Chen Q, Li G, Luo S, Song T, et al. (2014) Interface engineering of highly efficient perovskite solar cells. Science 345: 542-546.

10. Burschka J, Pellet N, Moon SJ, Baker RH, Gao P, et al. (2013) Sequential deposition as a route to high-performance perovskite-sensitized solar cells. Nature 499: 316-319.

11. Liu MZ, Johnston MB, Snaith HJ (2013) Efficient planar heterojunction perovskite solar cells by vapour deposition. Nature 501: 395-398.

12. Chen Q, Zhou H, Hong Z, Luo S, Duan HS, et al. (2013) Planar heterojunction perovskite solar cells via vapor-assisted solution process. J Am Chem Soc 136: 622-625.

13. Kim YH, Cho H, Heo JH, Kim TS, Myoung N, et al. (2015) Multicolored organic/inorganic hybrid perovskite light-emitting diodes. Adv Mater 27: 1248-1254.

14. Xing G, Mathews N, Lim SS, Yantara N, Liu X, et al. (2014) Low-temperature solution-processed wavelength-tunable perovskites for lasing. Nat Mater 13: 476-480.

15. Kagan CR, Mitzi DB, Dimitrakopoulos CD (1999) Organic-inorganic hybrid materials as semiconducting channels in thin-film field-effect transistors. Science 286: 945-947.

16. Hirasawa M, Ishihara T, Goto T, Uchida K, Miura N (1994) Magnetoabsorption of the lowest exciton in perovskite-type compound $(CH_3NH_3)PbI_3$. Physica B 201: 427-430.

17. Xie Z, Liu S, Qin L, Pang S, Wang W, et al. (2015) Refractive index and extinction coefficient of $CH_3NH_3PbI_3$ studied by spectroscopic ellipsometry. Opt Mater Express 5: 29-43.

18. LÖper P, Stuckelberger M, Niesen B, Werner J, Filipič M, et al. (2014) Complex refractive index spectra of $CH_3NH_3PbI_3$ perovskite thin films determined by spectroscopic ellipsometry and spectrophotometry. J Phys Chem Lett 6: 66-71.

19. Lin Q, Armin A, Nagiri RCR, Burn PL, Meredith P (2015) Electro-optics of perovskite solar cells. Nat Photonics 9: 106-112.

20. Chen CW, Hsiao SY, Chen CY, Kang HW, Huang ZY, et al. (2015) Optical properties of organometal halide perovskite thin films and general device structure design rules for perovskite single and tandem solar cells. J Mater Chem A 3: 9152-9159.

21. Xue SW, Zu XT, Zheng WG, Deng HX, Xiang X (2006) Effects of Al doping concentration on optical parameters of ZnO: Al thin films by sol-gel technique. Physica B 381: 209-213.

22. Xue S W, Zu XT, Zhou WL, Deng HX, Xiang X, et al. (2008) Effects of post-thermal annealing on the optical constants of ZnO thin film. J Alloy Compd 448: 21-26.

23. Yang A, Bao X, Li S, Yang R, Wang N, et al. (2014) Nano-ZnO film preparation at low temperature and the optical indices calculation. Optoelectron Lett 10: 216-220.

24. Bao X, Wang Y, Zhu Q, Zhu D, Wang J, et al. (2015) Efficient planar perovskite solar cells with large fill factor and excellent stability. J Power Sources 297: 53-58.

25. Yuvaraj D, Rao KN (2008) Optical and electrical properties of ZnO films deposited by activated reactive evaporation. Vacuum 82: 1274-1279.